tion from MC-simulated $e^+e^- \to \pi^- D^+ \bar{D}^{*0}$ three-body phase-space events. Here, also, the $\pi^- D^+$-tagged event sample that is used to study $\pi^- D^+ \bar{D}^{*0}$ includes some cross feed from the $\pi^- Z_c(3885)^+$, $Z_c(3885)^+ \to \bar{D}^0 D^{*+}$ signal channel, where the D^+ used for tagging is a decay product of the D^{*+}. The dashed histogram is from MC-simulated $e^+e^- \to \pi^- Z_c(3885)^+$, $Z_c(3885)^+ \to \bar{D}^0 D^{*+}$, $D^{*+} \to \pi^0 D^+$ events.

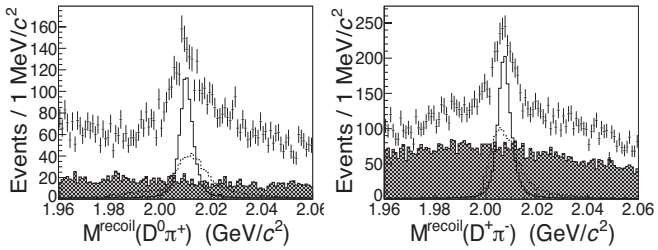

FIG. 1. The πD recoil mass distribution for the $\pi^+ D^0$- *(left)* and $\pi^- D^+$-tagged *(right)* events. Points with errors are data, the hatched histogram shows the events from the D mass sidebands. The solid and dashed histograms are described in the text.

We apply a two-constraint kinematic fit to the selected events, where we constrain the invariant mass of the D^0 (D^+) candidate tracks to be equal to m_{D^0} (m_{D^+}) and the mass recoiling from the $\pi^+ D^0$ ($\pi^- D^+$) to be equal to $m_{D^{*-}}$ ($m_{\bar{D}^{*0}}$). If there is more than one bachelor pion candidate in an event, we retain the one with the smallest χ^2 from the kinematic fit. Events with $\chi^2 < 30$ are selected for further analysis. For the $\pi^+ D^0$-tag analysis, we require $M(\pi^+ D^0) > 2.02$ GeV to reject the events of the type $e^+e^- \to D^{*+} D^{*-}$, $D^{*+} \to \pi^+ D^0$. The left (right) panel of Fig. 2 shows the distribution of $D^0 D^{*-}$ ($D^+ \bar{D}^{*0}$) invariant masses recoiling from the bachelor pion for the $\pi^+ D^0$ ($\pi^- D^+$) tagged events. The two distributions are similar and both have a distinct peak near the $m_D + m_{\bar{D}^*}$ mass threshold. For cross-feed events, the reconstructed D meson is not in fact recoiling from a $\bar{D}^*$ and the efficiency for satisfying these selection requirements decreases with increasing $D\bar{D}^*$ mass. Studies with phase-space MC event samples show that this acceptance variation is not sufficient to produce a peaking structure.

To characterize the observed enhancement and determine the signal yield, we fit the histograms in the left and right panels of Fig. 2 using a mass-dependent-width Breit-Wigner (BW) lineshape to model the signal and smooth threshold functions to represent the non-peaking background. For the signal, we use $dN/dm_{D\bar{D}^*} \propto (k^*)^{2\ell+1} |BW_{Z_c}(m_{D\bar{D}^*})|^2$, where k^* is the Z_c momentum in the e^+e^- rest frame, ℓ is the π-Z_c relative orbital angular momentum and $BW_{Z_c}(m_{D\bar{D}^*}) \propto \frac{\sqrt{m_{D\bar{D}^*}\Gamma_{Z_c}}}{m^2_{Z_c} - m^2_{D\bar{D}^*} - i m_{Z_c}\Gamma_{Z_c}}$. Here $\Gamma_{Z_c} = \Gamma_0 (q^*/q_0)^{2L+1} (m_{Z_c}/m_{D\bar{D}^*})$, where $q^*(m_{D\bar{D}^*})$ is the D momentum in the $Z_c(3885)$ rest frame, $q_0 = q^*(m_{Z_c})$ and L is the D-$\bar{D}^*$ orbital angular momentum. In the default fits, we set $\ell = 0$, $L = 0$ and leave m_{Z_c} and Γ_0 as free parameters. We multiply the BW by a polynomial determined from a fit to the MC-determined mass-dependent efficiency to form the signal probability density function (PDF). Mass resolution effects are less than 1 MeV/c^2 and, thus, ignored. For the non-peaking background for the $M(D\bar{D}^*)$ distribution, we use: $f_{\rm bkg}(m_{D\bar{D}^*}) \propto (m_{D\bar{D}^*} - M_{\rm min})^c (M_{\rm max} - m_{D\bar{D}^*})^d$, where $M_{\rm min}$ and $M_{\rm max}$ are the minimum and maximum kinematically allowed masses, respectively. The exponents c and d are free parameters determined from the fits to the data.

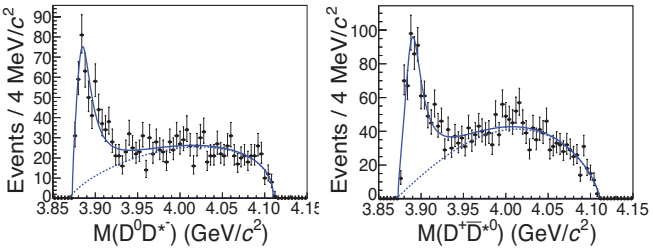

FIG. 2. The $M(D^0 D^{*-})$ *(left)* and $M(D^+ \bar{D}^{*0})$ *(right)* distributions for selected events. The curves are described in the text.

The results of the fits are shown as solid curves in Fig. 2. The dashed curves show the fitted non-resonant background. The fitted BW masses and widths from the $\pi^+ D^0$ ($\pi^- D^+$) tagged sample are 3889.2 ± 1.8 MeV/c^2 and 28.1 ± 4.1 MeV (3891.8 ± 1.8 MeV/c^2 and 27.8 ± 3.9 MeV), where the errors are statistical only. Since the mass and width of a mass-dependent-width BW are model dependent and may differ from the actual resonance properties [27], we solve for $P = M_{\rm pole} - i\Gamma_{\rm pole}/2$, the position in the complex (M, Γ) plane where the BW denominator is zero, and use $M_{\rm pole}$ and $\Gamma_{\rm pole}$ to characterize the mass and width of the $Z_c(3885)$ peak. Table I lists the pole masses and widths for the $\pi^+ D^0$ and $\pi^- D^+$ tagged samples.

TABLE I. The pole mass $M_{\rm pole}$ and width $\Gamma_{\rm pole}$, signal yields and fit quality (χ^2/ndf) for the two tag samples.

Tag	$M_{\rm pole}$(MeV/c^2)	$\Gamma_{\rm pole}$(MeV)	Z_c signal (evts)	χ^2/ndf
$\pi^+ D^0$	3882.3 ± 1.5	24.6 ± 3.3	502 ± 41	54/54
$\pi^- D^+$	3885.5 ± 1.5	24.9 ± 3.2	710 ± 54	60/54

Monte Carlo studies of possible sources of peaking backgrounds in the $D\bar{D}^*$ mass distribution show that processes of the type $e^+e^- \to D\bar{D}_X$, $\bar{D}_X \to \bar{D}^*\pi$, would produce a near-threshold reflection peak in the $D\bar{D}^*$ mass distribution, where D_X denotes a $D^*\pi$ resonance with mass near the upper kinematic boundary. This boundary, $\sqrt{s} - m_D$, is 30 MeV/c^2 below the mass of the lightest established $D^*\pi$ resonance, the $D_1(2420)$,